

# Low Pressure Schlieren Imaging of a Multi-Stream Injection Nozzle

Adam M. Ragheb<sup>1</sup> and Gregory S. Elliott<sup>2</sup>

*University of Illinois at Urbana-Champaign, Department of Aerospace Engineering, Urbana, IL 61801*

Darren King<sup>3</sup>, Julia Laystrom-Woodard<sup>4</sup>, David L. Carroll<sup>5</sup> and Wayne C. Solomon<sup>6</sup>  
*CU Aerospace L.L.C., Champaign, IL 61820*

The mechanisms of the mixing between separate flows are of high interest in order to increase the efficiency of processes that rely on well mixed flows. Mixing of three flows was examined, where two of the flows were in an underexpanded state, and the third near-ideally expanded. One of the underexpanded flows served as a driver gas for the mixing of the remaining two streams, and it was the ejector nozzles of this flow whose geometry was examined with the goal of passively enhancing its driving capability of the mixing of the remaining two flows. From previous planar laser induced fluorescence images it was concluded that small starletted cylinders exhibited the highest degree of mixing, as the starlets created large-scale structures that helped to entrain the flows into one another. Starlets also improved the mixing of large cylindrical ejectors, but not as efficiently as was the case for the small starletted cylinders. Thus, the small starlets effectively maximized both the diffusive and convective aspects of fluid mixing. In this study, schlieren imaging techniques were employed to determine and document the properties and structure of the supersonic flow, yielding descriptive images of the barrel-shaped shocks, expansion waves, and other supersonic flow features at low pressures between 6.6 and 17.5 torr.

## Nomenclature

COIL	=	chemical oxygen iodine laser
mmol/s	=	millimoles per second
SE	=	slot-ejector
SEI	=	slot-ejector-injector

## I. Introduction

The mechanisms of the mixing between separate flows are of high interest in order to increase the efficiency of processes that rely on well-mixed flows. Two of these areas are combustion, and chemical oxygen-iodine lasers (COILs). It is widely known that as the speed of two flows increase, the shear, or mixing layer between the two flows narrows. Initially, this observation was attributed to density effects, as an increase in Mach number brought with it a decrease in temperature, and thus an increase in the fluids' density. Brown and Roshko<sup>1</sup> examined the effects of density in turbulent mixing layers, determining that while density plays a small role, the effects of compressibility play a much larger role in determining the mixing rate of high speed flows. These compressibility effects were quantified by Papamoschou and Roshko<sup>2</sup> and named the convective Mach number. This convective Mach number is the Mach number of the flow in a frame of reference that moves at the velocity of the large-scale mixing structures of the flow.

---

<sup>1</sup> Graduate Research Assistant, AIAA Student Member.

<sup>2</sup> Professor, AIAA Associate Fellow.

<sup>3</sup> Senior Laboratory Manager, AIAA Member.

<sup>4</sup> Senior Engineer, AIAA Member.

<sup>5</sup> Vice President and COO, AIAA Associate Fellow.

<sup>6</sup> President, AIAA Fellow.

Using the above concepts, a number of studies have been performed with the goal of enhancing the mixing of high speed flows. Yu and Schadow<sup>3</sup> investigated the use of a resonant cavity installed immediately downstream of a circular jet, and were able to demonstrate a threefold increase in the spreading rate of the shear layer at a convective Mach number of 0.85. Gilinsky and Seiner<sup>4</sup> investigated the use of corrugated nozzles on a converging-diverging nozzle with a design Mach number of 1.5. Using CFD, a 4dB acoustic benefit and a 1% increase in thrust was demonstrated, with both of these results attributed to better mixing between the flows through and around the jet. Kim and Samimy<sup>5</sup> studied trailing edge modifications of rectangular jets. By locating simple cutouts at the nozzle exit, the area of the shear layer was up to doubled. This significant increase in the mixing area was attributed to the shedding of streamwise vortices from the modified trailing edges, and was most prominent for the case of an underexpanded nozzle.

Nikolaev and Zagidullin<sup>6</sup> proposed and tested an advanced nozzle arrangement for application in COILs, consisting of an array of slots, ejectors, and injectors. Vertical arrays of cylindrical ejectors alternated with rectangular slots. Each of the cylindrical ejector arrays were flanked by a pair of injector tubes, each of which had numerous round perforations. This concept was based on using the flow from the ejectors to mix the flows emanating from the slots and injectors. It was hypothesized that the expansion of underexpanded gas from adjacent ejector arrays would create an aerodynamic throat of sorts, compressing the slot and injector flows into one another and forcing them to mix. With this nozzle arrangement, Nikolaev observed gas temperatures lower than would be expected from expansion alone, and a stagnation pressure of the non-ejector flows significantly higher than the slot plenum pressure and the stagnation pressure of the injector flows. This increased stagnation pressure was therefore attributed to a transfer of momentum to these flows from the ejector flow. The observed distance of mixing was much shorter than that which was estimated based of molecular diffusion coefficients; this result, along with the decreased temperature and increased stagnation pressures were all desirable characteristics for COIL nozzle designs. Better understanding and future improvements to the arrangement of Ref. 6 requires knowledge of the details of the flow downstream of the slots, ejectors, and injectors.

Based on the observations and theory of Ref. 5 and proposed by D. Carroll and W. Solomon<sup>7</sup>, the addition of “starlets” is hypothesized to create streamwise vorticity, which would further enhance the mixing between the slot and injector flows. This increased vorticity would work with the existing large scale mixing structures shed from the ejectors to increase the growth angle of the shear layer between the flows, thus improving the mixing, and aiding the fields of combustion and COILs, to name a few. Herein we used schlieren photography at low pressures to evaluate the general compressible flow features of an arrangement of slots, ejectors, and injectors based on the baseline case of Ref. 6 and the starlet configurations discussed by Ragheb *et al.*<sup>8</sup> The flow conditions would be similar to that baseline case, and would also test candidate starletted ejectors. The goal of this paper is to describe the flow features downstream of a baseline slot, ejector, and injector arrangement and downstream of an arrangement with improved ejectors to determine their effects.

## II. Slot, Ejector, and Injector Block Design

The general arrangement proposed by Ref. 6 was used for the slot-ejector-injector (SEI) block, with large and small cylindrical ejectors, both plain and starletted, for a total of four geometries. A diagram of the ejector block with the three slots, four ejector columns, and six injector tubes labeled, is presented in Figure 1. This ejector block will henceforth be referred to as the SEI block.

As described in Refs. 6 and 8, the reasoning behind the design of this configuration is to greatly facilitate the mixing between the flows emanating from the injectors and the slots at higher total pressures. The ejector flow is at a very high pressure, exiting the ejectors at a Mach number of unity and in an underexpanded state.

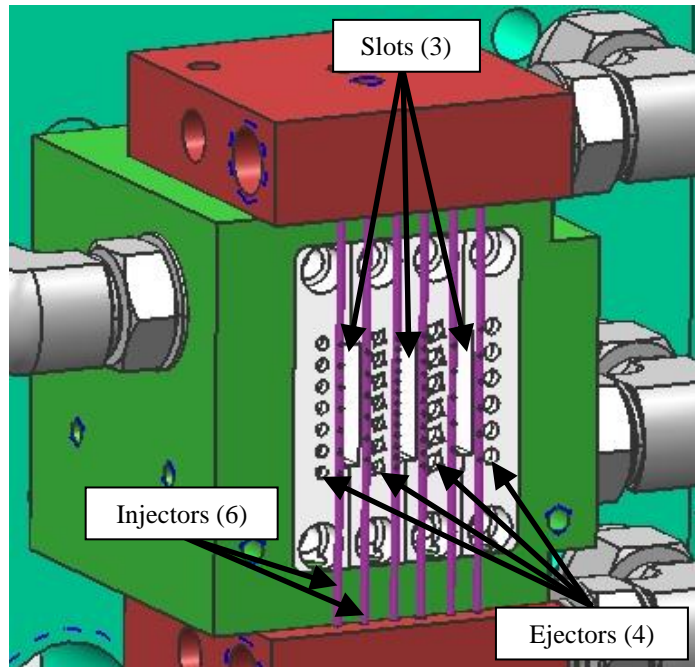


**Figure 1. Diagram of the slot-ejector-injector (SEI) configuration with all ejector geometries.**

The slot flow, due to the large cross-sectional area of the slot and the relatively low flowrate, exits the slots at a subsonic speed and very near a properly-expanded state. The injector flow, like the ejector flow, exits the injectors in an underexpanded state, at a Mach number of, or very near to, unity. Immediately downstream of the block face, the high-pressure ejector flow expands and compresses the flows of both the slot and injector flows while forcing the injector flow into the slot flow. The redirection of the injector flows on both sides of the slot forms an aerodynamic throat (Fig. 2) that accelerates the slot flow to a Mach number of unity<sup>6,8</sup>.

The schematic of Figure 2 views the SEI block parallel to the injector and ejector columns, and is the perspective that will hereto be referred as the “90 Degree-Rotated Orientation;” rotating the SEI block 90 deg. yields the “Standard Orientation” of the schlieren imaging.

Figure 3 provides a photograph of the four ejector geometries tested with the two imaging orientations referenced. The upper left section depicts the large cylinder configuration, where the six cylindrical holes have a diameter of 0.198 cm and are spaced 0.320 cm center-to-center. The lower left section depicts the small cylinder configuration, where the seven cylindrical holes have a diameter of 0.147 cm and have a center-to-center measurement of 0.264 cm. The upper right section depicts the large starlet configuration, and the lower right section depicts the small starlet configuration. For all four of the slot-ejector (SE) configurations, the three nitrogen slots each measured 1.501 cm tall by 0.249 cm wide. The starlets are simply cylindrical ejectors with four notches cut into the ends at the exit of the cylinders.

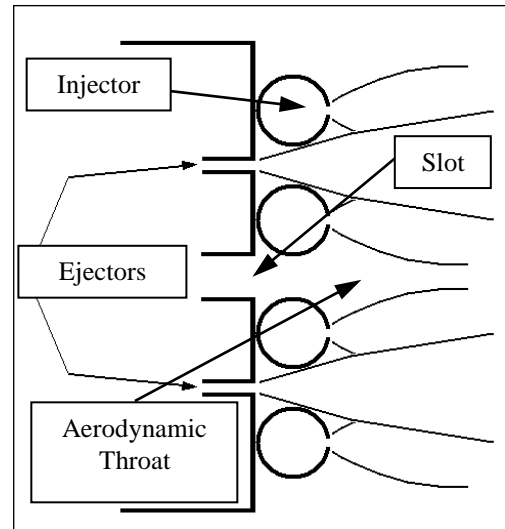


Figure 2. SEI schematic and pressure-based near-field flow interaction.

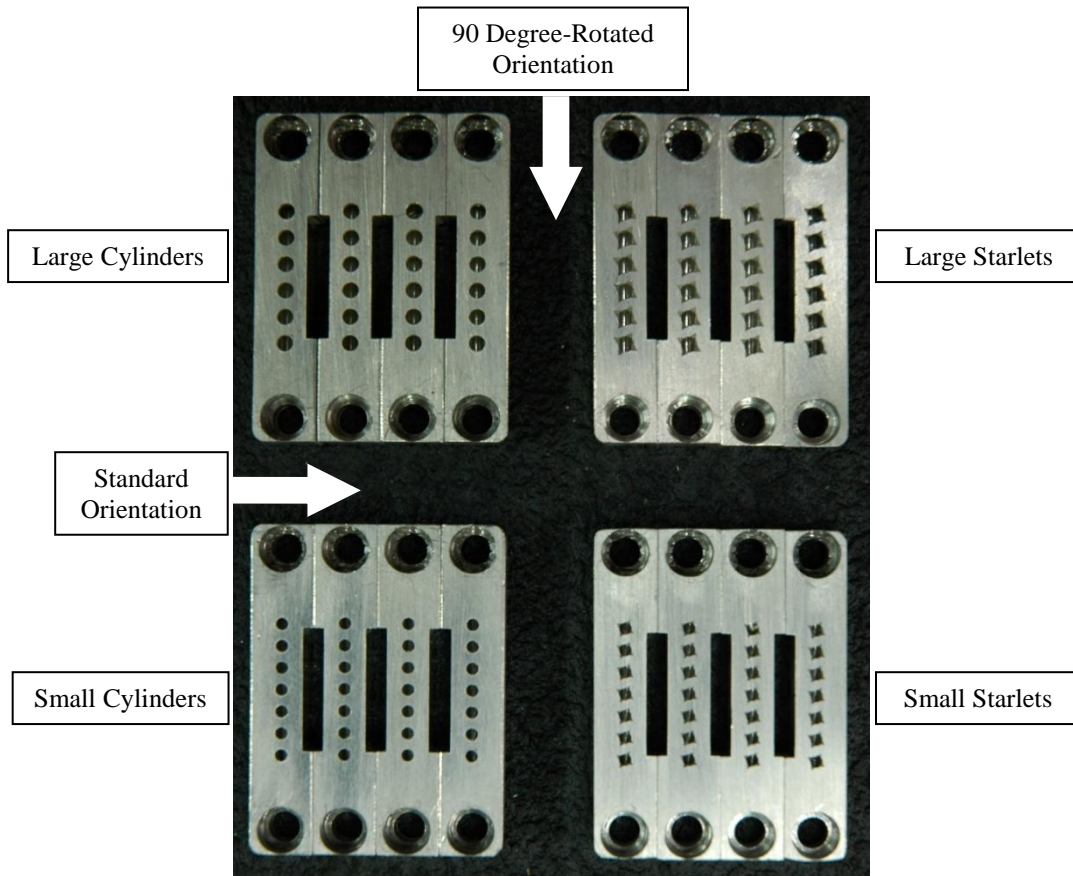


Figure 3. Image of the four slot-ejector (SE) configurations tested.

### III. Experimental Setup and Configuration

The schlieren images of this study were recorded with a PCO 1600 digital camera with 1 gigabyte of RAM outfitted with a Nikon Nikkor 70-300 mm zoom lens. A Quantum Composer 9518 pulse generator was used to create a 10 Hz signal that simultaneously activated the General Radio 1538-A Strobotac strobe light controller and pulsed the PCO 1600 digital camera to acquire an image. Images were transferred

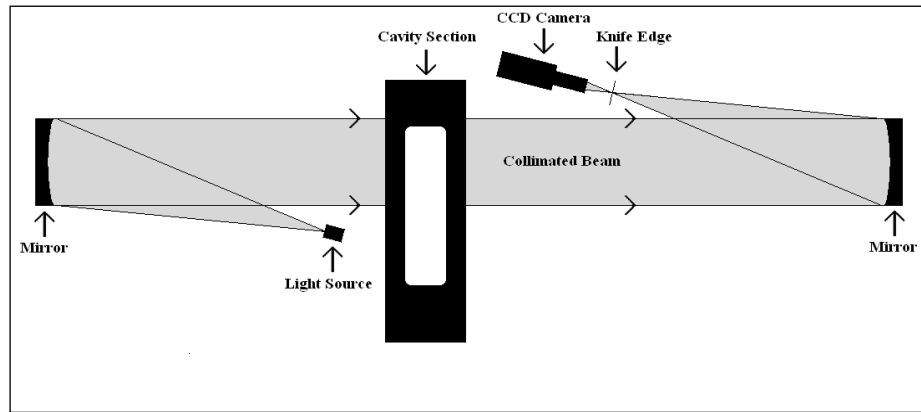


Figure 4. Diagram of schlieren imaging setup.

between the digital camera and a PC by way of a USB cable. A Tektronix TDS 2024B four-channel digital storage oscilloscope was used to verify the synchronization of the strobe light and camera, as well as to determine a reasonable exposure time for the camera. The exposure time of 10 milliseconds (ms) was set using the PC. Figure 4 provides a diagram of the experimental schlieren imaging setup.

As depicted in Figure 4, the schlieren imaging setup involved the light from the Strobotac strobe light being reflected in a collimated beam through the cavity section. In order to yield a beam of collimated light, the strobe light was placed at the focal point of the mirror that was reflecting it through the cavity section. Once it passed through the cavity section and the density gradients and shockwaves of the flow that were being examined, another mirror was used to redirect the beam toward the PCO 1600 CCD camera. Located at the focal length of this second mirror was a knife edge, and approximately 5 cm behind that was the front of the lens of the camera. The knife edge was adjusted so as to block approximately half of the light, allowing the density gradients of the flow to become readily visible. Arrows in Figure 4 depict the path of the light from the light source, through the cavity, past the knife edge, and finally into the lens of the camera. The strobe light, digital camera, and cavity section are pictured in Figure 5. Two things should be noted at the outset of this investigation. First that the schlieren technique is a “line of sight” flow visualization, which combines the effects as the light passes through the test section. Secondly, the data shown here are qualitative and it is often difficult to accurately determine the types of waves generated. In the present case interpreting the images and waves produced is done based on a comparison with other non-pressure matched jets and due to the more complex flow field it is subjective.

The test section, or cavity, used for this experiment was square and had a constant cross-sectional area, with an equal internal height and width of 12.7 centimeters (cm). The cavity was 40.6 cm long, and had ports on all four sides that enabled the rapid access to the interior of the section for pressure measurements; the cavity dimensions were selected to fit the slot-ejector-injector (SEI) block of Refs. 6 and 8.

The cavity was milled from a square piece of Aluminum and was anodized matte black for corrosion

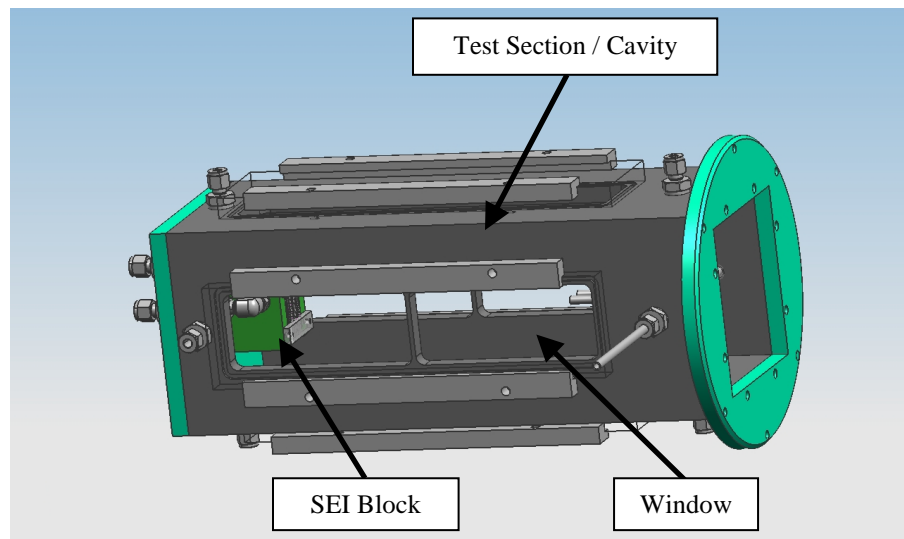


Figure 5. Cavity with SEI block and windows labeled.

protection as well as to reduce reflection and scattering of light. The cavity had four large openings that were fitted with removable windows. For this series of tests, these windows were 0.635 cm-thick glass plates, affixed to the cavity with two aluminum window retainers each, and sealed with a rubber O-ring. One of these windows is visible in Figure 5.

The main component of the vacuum system was a Kinney KT-850 single-stage rotary vacuum pump driven by a 50 HP electric motor, with an MD-90 Roots blower, powered by a 5 HP motor, installed in series with the pump. These two components were connected to one another by a 20.3 cm diameter vacuum pipe, and combined, the two have the ability to pump a total of approximately 1100 litres per second, with the exhaust exiting through a 10.2 cm diameter PVC pipe. When utilized together and with no flow present, pressures of around 0.5 torr could be achieved in the cavity<sup>9</sup>.

Pressure measurements were acquired using one PX212-200AV, one PX212-060AV, and various PX319-015AV pressure transducers manufactured by Omega Engineering, with absolute ranges of 200, 60, and 15 psia, respectively. The 200AV and 060AV transducers were used to monitor the upstream ejector feed and the upstream slot flow, respectively, while the -015AV transducers were used to measure cavity pressures. All transducer output signals were routed to a National Instruments (NI) TBX-1303 32-channel DAQ board, which in turn was connected to an NI SCXI-1000 slot chassis by way of a SCXI-1102 32-channel input module. Communication between an HP PC and the SCXI-1000 slot chassis was achieved through the utilization of a SCXI-1600 DAQ and control module that converted the signals to a USB 2.0 output. LabVIEW 8.0 was installed and used on the HP PC to run the pressure-reading vi.

Flow measurements were taken with two Micro Motion Elite CMF025H and one CMF010H Mass Flow Sensors. These sensors are capable of maximum flow rates of approximately 42,000 and 2,000 mmol/s, respectively. One sensor each was installed in line with the slot, ejector, and injector flows, and preexisting calibrations were used for each different gas.

For these experiments, the baseline case was very similar to the baseline case studied by Refs. 8 and 10. Our baseline flowrates were 32.1 mmol/s through the slots, 686 mmol/s through the ejectors, and 6.9 mmol/s through the injectors, with all three flows being pure Nitrogen. In order to determine whether the flow structure changed significantly for different ejector flowrates, we also ran ejector flowrates of 400, 200, and 0 mmol/s. Finally, and in order to uncomplicate the flowfield, test cases were run with no injector flow

The cavity pressures at which these schlieren images were taken are summarized in Table 1. The majority of the data were taken at an ejector flowrate of 686 mmol/s corresponding approximately to the flow conditions of Nikolaev. At this highest ejector flowrate, the cavity pressure was consistently less than 18 torr.

**Table 1. Average Schlieren Cavity Pressures for Both the Large and Small Ejector Geometries**

Ejector Flowrate (mmol/s)	Cavity Pressure (torr)	
	Large	Small
<b>686</b>	17.3	17.6
<b>400</b>	11.5	11.9
<b>200</b>	6.4	6.7
<b>0</b>	2.1	2.4

#### IV. Experimental Results

The four ejector geometries were imaged at ejector flowrates of 686, 400 and 200 mmol/s, and slot flowrates of 0 and 32.1 mmol/s; for the sake of brevity, only the 32.1 mmol/s slot flowrate cases are presented here. These geometries were small and large cylinders, small and large starlets. For all geometries, the injector flowrate was constant at 6.9 mmol/s unless otherwise noted. The images were acquired at a rate of 10 Hz and the exposure time was approximately 10  $\mu$ s.

Acquiring schlieren data at low pressures is difficult, since at such a low gas density, the index of refraction changes are not very large. In order to optimize the acquired images, the images must go through digital post-processing that increases the contrast levels and eliminates the small index of refraction changes caused by the mediums and optics themselves. As visible in Eq. 1, the first post-processing step involves subtracting the background, which serves as a sort of unsharp masking, serving to remove variations in the indices of refraction not caused by the flowfield features<sup>11</sup>. Dividing this result by the flat-field, also having had unsharp masking previously applied to it, serves as a sort of contrast stretching, allowing the brightest pixels to become brighter, and the darkest pixels to become darker, and enhancing the contrast of the desired flow features<sup>11</sup>. This contrast enhancement

greatly improves the quality of the image, and allows for a large amount of qualitative data to be discerned by the human eye.

The flowfield, flat-field, and background images were recorded in stacks of 200, and the images processed according to

$$\text{Processed Image} = \frac{\text{flowfield} - \text{background}}{\text{flat-field} - \text{background}} \quad (1)$$

The flowfield image, as the name suggests, was recorded with the flows on, and the strobe light activated, while the flat-field image was recorded with the strobe light activated but no flow present. In order to increase the signal to noise ratio, the background image, taken with no flow and an inactive strobe light, was subtracted from both the flat-field and flowfield images. With the background subtracted from both the flowfield and the flat-field images, the result from the flowfield was then divided by the result of the flat-field to eliminate the noise inherent to the CCD camera. The extreme downstream portion of the image was then cropped out, as this investigation was concerned only with determining the early stages of the flowfield. An example of a before-and-after is presented below in Fig. 6; the unprocessed image is located on the left, while the processed image is located on the right. Figure 6 clearly validates the image post-processing technique used in these experiments, as the right-hand, processed image clearly depicts density gradients, while the left-hand, unprocessed image has no density gradients visible.

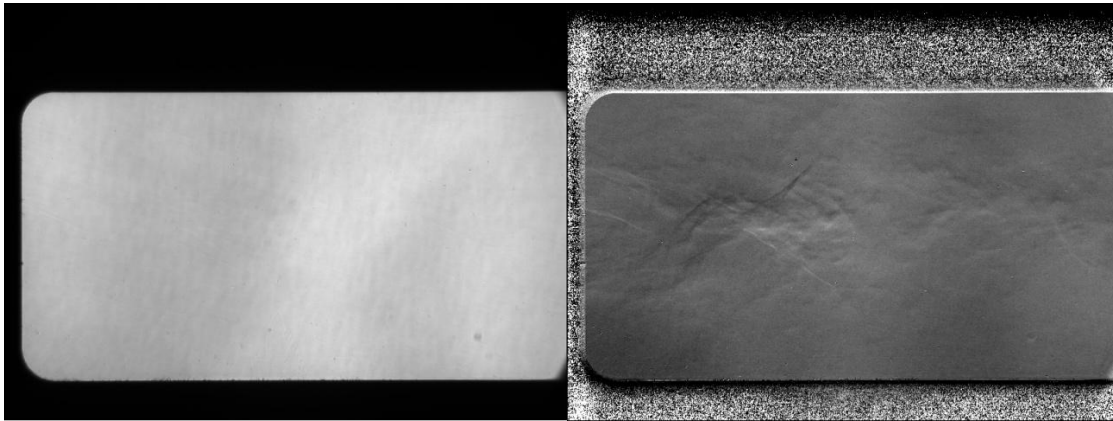


**Figure 6. Unprocessed (left) and processed (right) sample schlieren images.**

#### **A. Baseline Case**

Figure 7 depicts schlieren images generated from the large cylinder geometry at ejector flowrates of 686, 400, and 200 mmol/s, a slot flowrate of 32.1 mmol/s, and an injector flowrate of 6.9 mmol/s. The ejector flowrate is 686 mmol/s for the top two images, 400 mmol/s for the middle row, and 200 mmol/s for the bottom row of images, with the instantaneous images on the left-hand side of the page, and an image averaged over the 200 frames on the right-hand side. The point of view is that of the “Standard Orientation” as listed in Fig. 3. Additionally, Fig. 7 contains markings for the six ejector locations, approximated with small solid black lines to the left of each image.

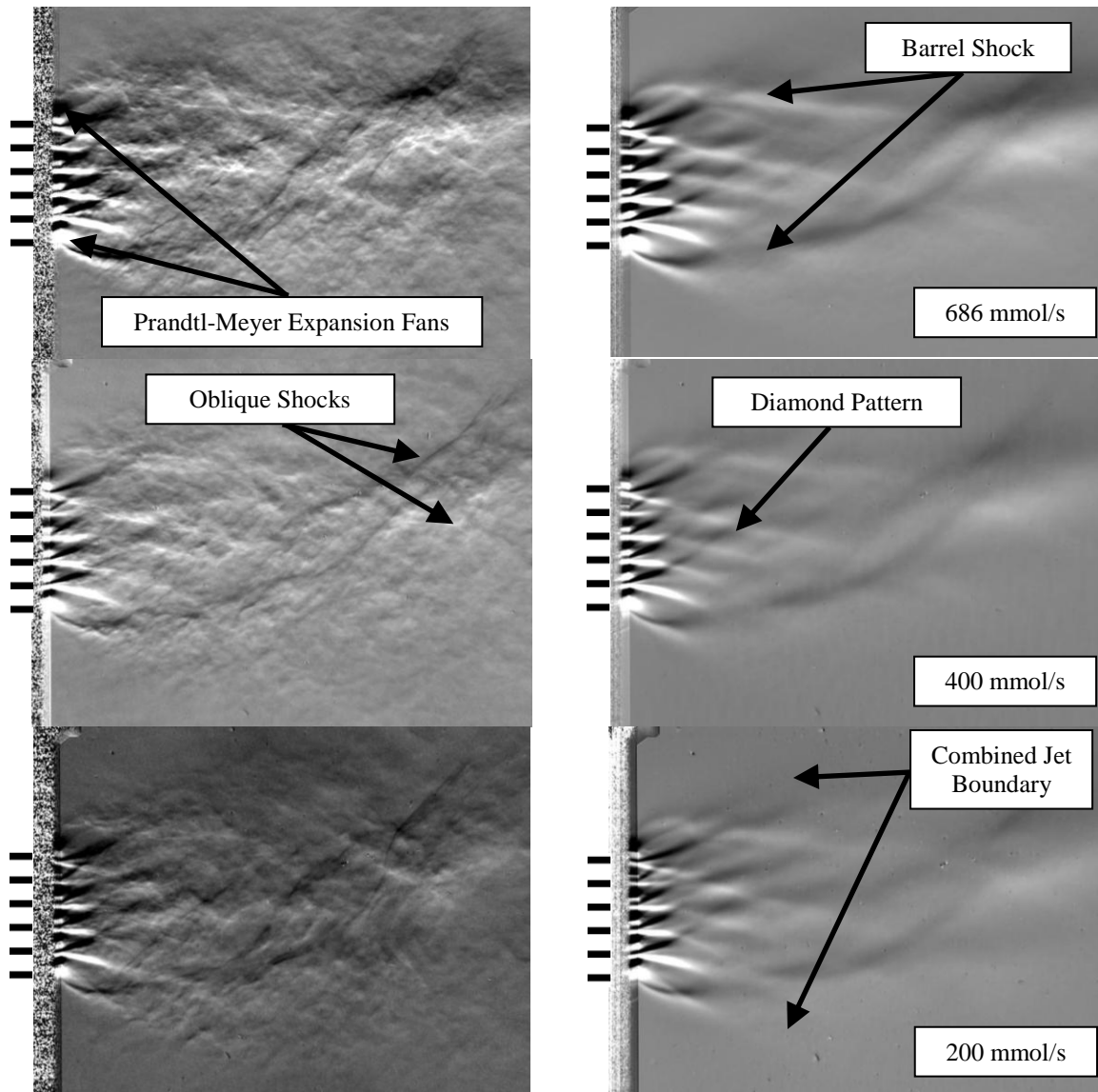


**Figure 7. Large cylinder instantaneous and averaged schlieren images at ejector flowrates of 200, 400, and 686 mmol/s with the six ejector locations approximated with small solid black lines to the left of each image; all flows present. Image covers an approximate area of 5.0 cm by 6.8 cm.**

Very strong density gradients, evidence of Prandtl-Meyer expansion fans, were observed near the ejector block face, within approximately the first 1.2 cm and these structures appeared to be very consistent in time as evidenced by the minute differences in these structures when comparing the instantaneous and averaged images. These expansion fans support the fact that the ejector flows were highly-underexpanded when they exited the ejectors, as the gradients expanded outward as opposed to contracting inward, the latter of which would suggest an overexpanded flow condition. At the top and bottom edges of the ejector columns, the expansion fans were readily visible due to a lack of adjoining ejectors, and they are labeled in Fig. 7. Approximately 0.7 cm downstream of the face, the weak shocks from the ejectors interacted and intersected with one another, forming an intricate diamond-shaped pattern. Bounded by the top and bottom ejectors, and extending approximately 4.7 cm downstream of the face, a barrel shock was readily visible in the averaged images as a result of the focusing and merging of the weak shocks and the vacuum pump creating a strong lower pressure gradient for the flow to move from the ejector block toward the downstream end of the cavity. Outside of the boundaries of the barrel shock, the combined jet boundary was visible, and is the shear layer between the combined jet and the undisturbed regions of the cavity. At the downstream end of the shock, there existed a pair of oblique shocks; the Mach disk that, according to Ref. 12, would

be expected at the downstream end of the barrel shock was not apparent in this orientation. The pair of oblique shocks was more pronounced than the barrel shock, and was readily visible in even the instantaneous images.

As the flow velocity was decreased from the baseline flowrate of 686 mmol/s to 400 and 200 mmol/s, respectively, some changes were noted. The density gradients decreased in their size and intensity, as would be expected with lower flowrates. Specifically, the strength of the barrel shock decreased with decreasing ejector flowrate. Notable consistencies despite the changes in ejector flowrate include the general structure of the flow, and the length of the barrel shock. These facts show that the general structure and flow interactions are not flowrate dependent over the range of 686 to 200 mmol/s, and thus a minor change in the flowrate over this range will not change the general flow structure.

Looking in the downstream direction from behind the ejector plate, the ejector block was rotated 90 degrees counterclockwise for all of the 90 degree-rotated orientation schlieren images; this point of view is labeled in Fig. 3. Aside from this change, the balance of the equipment settings and test conditions were identical. Figure 8 depicts schlieren images generated from the large cylinder geometry at ejector flowrates of 686, 400, and 200 mmol/s in the top, middle, and bottom rows, respectively. A diagram is located on the left-hand side of each image, with grey indicating the location of slots, black indicating ejectors, and white and black vertical stripes indicating injectors. The injector flowrate was 6.9 mmol/s for these cases, and the slot flowrate was 32.1 mmol/s. As was to be expected, and in agreement with Nikolaev's SEI block design, the ejector flows and injector flows, when present, were highly underexpanded upon their exit from the SEI block.

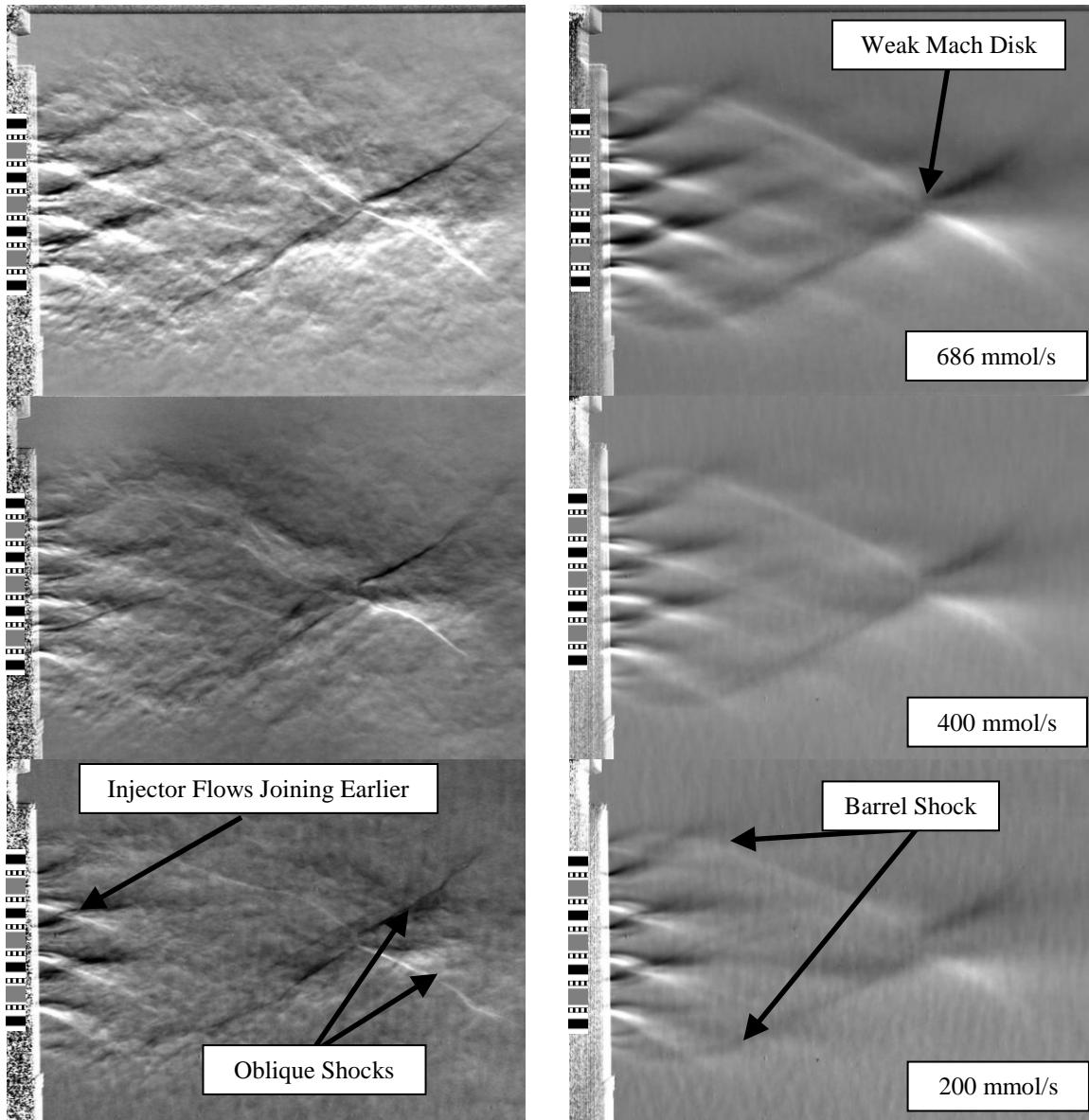


**Figure 8. Large cylinder instantaneous and averaged schlieren images at ejector flowrates of 200, 400, and 686 mmol/s; ejector block rotated 90 degrees, all flows present. Image covers an approximate area of 4.8 cm by 6.6 cm.**

For all three ejector flowrates, a very distinct pair of oblique shocks was visible in both the instantaneous and averaged images with a half angle of approximately 27.5 degrees, indicating a Mach number of 2.0. As was to be expected, the intensity of these shocks diminished as the ejector flowrate decreased from 686 to 200 mmol/s. The location of this pair of shocks did not change with the flowrate, remaining approximately 6.4 cm downstream of the ejector face. Unlike the standard orientation of Fig. 7, this flow remained centered in the plane of the image when the slot flow was not present. A barrel shock with its associated outer shear layer<sup>13</sup> was visible; however it narrowed and closed much quicker than in the standard orientation case, very possibly due to the slot dimensions in each orientation. Once again, a series of interconnected diamond-shaped shock / expansion waves were visible, and were more well-defined than in the orientation of Fig. 7. This was due to the fact that the distance between the columns of ejectors was significantly larger than the separation between two adjacent ejectors in the same column, allowing for the Prandtl-Meyer expansion fans to be less affected and confined by the neighboring ejector column than they were by the ejector above or below a given ejector. It cannot be determined with certainty whether

interconnecting structures are shocks or expansion fans due to the complex flow structure, but we believe that these structures most closely correspond to the intercepting shock of Ref. 13.

One notable change observed as the flowrate decreased, was a widening of the region where a Mach disk would be expected to reside; this area is located at the downstream end of the barrel shock and the upstream end of the oblique shock pair. Another change observed was that the series of interconnected shock / expansion waves, while visible over nearly the entire length of the barrel shock for the 686 mmol/s case, reduced in intensity and shortened as the ejector flowrate was decreased. As a result, the aerodynamic throat as depicted in Fig. 2 was shortened and widened as the ejector flowrate was reduced, decreasing its effectiveness. This shortening of the shock / expansion waves is deduced from the fact that adjacent injector flows met earlier as the ejector flowrate was decreased, and follows with the theory of Ref. 6, which states that the expansion of the underexpanded ejector flows is what creates an aerodynamic throat downstream of each of the slots.

### B. Large Cylinder Cases

Figure 9 depicts the schlieren images from the large ejectors at an ejector flowrate of 686 mmol/s, a slot flowrate of 32.1 mmol/s and an injector flowrate of 0 mmol/s; the cylinders are located in the top row, and the starlets in the bottom row. An instantaneous image is presented on the left side, while a 200-image average is presented on the right. Solid black lines give the approximate ejector locations, while the alternating white and black vertical lines locate the off-centered injectors.

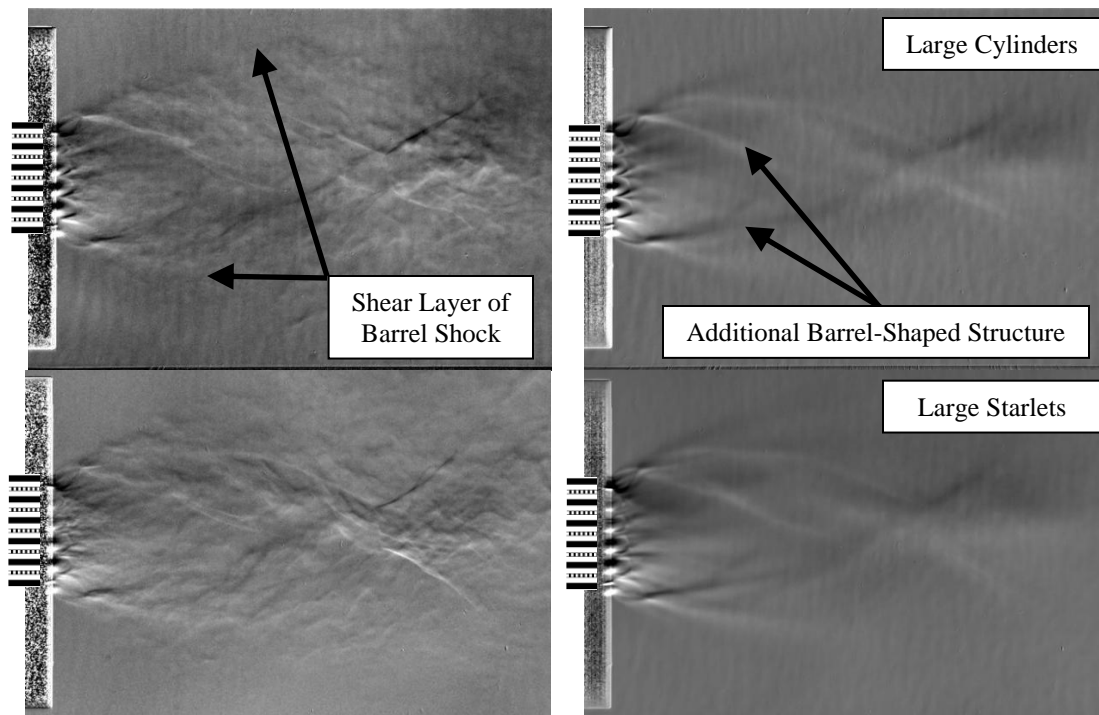


**Figure 9. Large cylinder (top) and starlet (bottom) instantaneous (left) and averaged (right) schlieren images, no injector flow. Image covers an approximate area of 5.5 cm by 8.0 cm.**

A comparison between the instantaneous and averaged images of Fig. 9 exhibited similar flow features between the two. A barrel shock with its associated outer shear layer<sup>14</sup> was present in both, being wider and extending further downstream when the slot flowrate was 32.1 mmol/s. This slot flowrate also resulted in a stronger pair of oblique shocks, the top one of which was visible even in the instantaneous image. In the no-slot flow example, omitted for brevity, two sets of weak shocks were visible emanating from the ejector block; they were the flows from the injectors and ejectors. The addition of the slot flow greatly shortened the triangular pattern of visible weak shocks by approximately 60%, and all but removed the longer set of weak shocks; this suggests that the slot flow entrains the ejector flow, mixing with it, and thus significantly reducing the density gradients. The slight degradation of the smaller set of expansion fans implies increased mixing of the flows with the injector flow. As was the case in Fig. 7, the flow was observed to be deflected slightly upward, with the effect mitigated slightly

through the addition of the slot flow. Another result of the addition of the slot flow was a second, smaller barrel-shaped structure as depicted in Fig. 9.

The same general flow structure was observed for the large starlets as was observed for the large cylinders, but the interlocking triangle pattern of weak shock of the averaged image appeared less defined, indicating shallower density gradients. This pattern is believed to have been created by weak shocks extending downstream of the intercepting shocks of each of the individual underexpanded jets of the nozzle. These weak shocks were more visible in the orientation of Figs. 10 and 12. Additionally, the top part of the large barrel shock and the top shock of the oblique shock pair appeared more blurred for the starlets, suggesting that these structures were less stable and varied in time to a greater degree as a result of the addition of the starlets. This is an indication of better mixing. The entire flow structure of the starlets appeared to be marginally shorter, with a slightly larger angle between the shocks, suggesting a lower exit velocity. This may have been due to a minor variation in the flowrates, but also may be attributed to the increased exit area of the starlets allowing for the ejector flow to be less underexpanded for the starlets than it was for the cylinders. The final piece of qualitative evidence supporting better mixing with the starlet geometry was the larger separation between the oblique shocks at the location where a Mach disk would be expected. As observed in Fig. 8, a larger oblique shock separation was associated with a lower ejector flowrate, which implied a lower overall average flow velocity once expanded. Since the mass flowrates of Fig. 9 are nearly identical, a slower downstream flow from the starlets implies increased mixing of the ejector flow with that of the slower injector and slot flows.

It should be noted that when comparing the density gradients visible in the standard orientation (the orientation viewed by the laser mirrors<sup>15</sup>), and the 90-degree rotated orientation, the density gradients viewed in the standard orientation were much less severe than those that were observed in the 90-degree rotated orientation which is presented in Figs. 10 and 12.

Figure 10 depicts the schlieren images from the large cylinders and starlets rotated 90 degrees at an ejector flowrate of 686 mmol/s, a slot flowrate of 32.1 mmol/s and an injector flowrate of 0 mmol/s. The arrangement of the cases is the same as that of Fig. 9. Once again, grey indicates the location of slots, black indicates ejectors, and white and black vertical stripes indicate the location of the injectors.

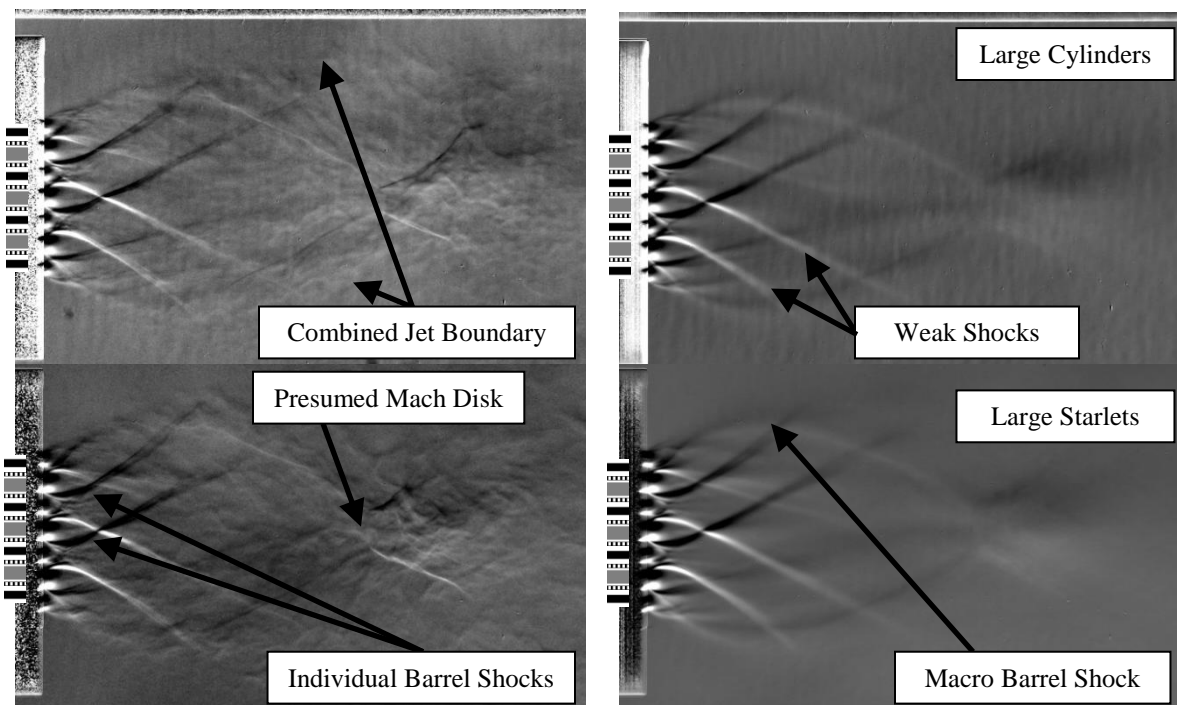


**Figure 10. Large cylinder (top) and starlet (bottom) instantaneous (left) and averaged (right) schlieren images; ejector block rotated 90 degrees, no injector flow. Image covers an approximate area of 5.5 cm by 9.0 cm.**

While not shown for brevity, a very well-organized density gradient pattern was created by the flow of only the ejectors. The downstream oblique shock pair and the barrel shock extending from the ejector face to the oblique

shock pair were readily visible in both the instantaneous and averaged images with a half angle of 32.5 deg., suggesting a Mach number of 1.66. The four columns of ejectors were also readily discernable in both the instantaneous and averaged images. The deletion of the injector flows, when compared to Fig. 8, stabilized all six weak shocks created by the individual intersecting shocks that existed on both edges of the three slots. These shocks were present, yet rather unstable for all flowrates of Fig. 8, but very well-defined and thus stabilized in Fig. 10. Evidence of their high level of stability is given by the existence of almost no observable change in their appearance between the instantaneous images of the left column to the 100-image averaged images of the right column.

It should be noted that examining the images from the 0 mmol/s slot and injector flowrate (not pictured), the expansion of the ejector flow created a very geometric and straight pattern of interlocking diamonds of weak shocks with a stable oblique shock pair existing downstream; the addition of the slot flows significantly destabilized the downstream pair of oblique shocks, suggesting the slots' shedding of large scale structures that destabilized the downstream flow. While they were easily recognizable in the instantaneous image, the blurriness and wide area of dark and light color indicates that this pair was not stable in time once the slot flow was added. Thus the addition of the slot flow has the effect of significantly reducing the density gradients in the mixed flow downstream.

As was to be expected, the same general structure, including the expansion waves, the barrel shock, the downstream oblique shock pair, and the combined jet boundary were visible in the large starlet images. Not very much changed in this orientation between the cylinder and starlet ejector geometries. The one main difference between the two flows was that in the averaged image with slot and injector flows present, the oblique shock pair appeared to have been more separated at its leading through the addition of starlets at the location where a Mach disk would be expected to reside<sup>12</sup>; this is visible for both the instantaneous and averaged images. Compared to the case of the large cylinders, the separation between the two points where the barrel shock ended and the oblique shock pair began for the large starlets was larger. This in itself could not be utilized to prove better mixing, but it could be used to support that fact; more mass is being channeled down the center of the flow at a lower velocity than without the starlets, thus forcing the two shocks to be spaced further apart.

In addition to the above observations, the individual underexpanded jets of this nozzle arrangement were seen to exhibit the characteristic intercepting shocks and curved jet boundaries of an underexpanded jet immediately downstream of the jet exit. These structures were more clearly identified for the cases shown in Figs. 10 and 12. The individual intercepting shocks extended downstream into the flow as weak shocks; these intercepting shocks were created from the individual Prandtl-Meyer expansion fans at the exit of each ejector.

The fact that nearly no change was observed in the shape and fineness of the weak shocks of the individual ejectors suggests that the addition of the starlets to the large ejectors did not significantly aid in the mixing of the ejector and slot flows in this axis. Since the top and bottom ejectors are located above the top and bottom boundaries of the slots, respectively, the slots would tend to minimally affect these flow structures.

### C. Small Cylinder Cases

Figure 11 depicts the schlieren images from the small cylinders and starlets in the arrangement introduced for Fig. 9, with the six injector and seven ejector locations diagrammed with alternating white and black vertical stripes and horizontal black lines, respectively.

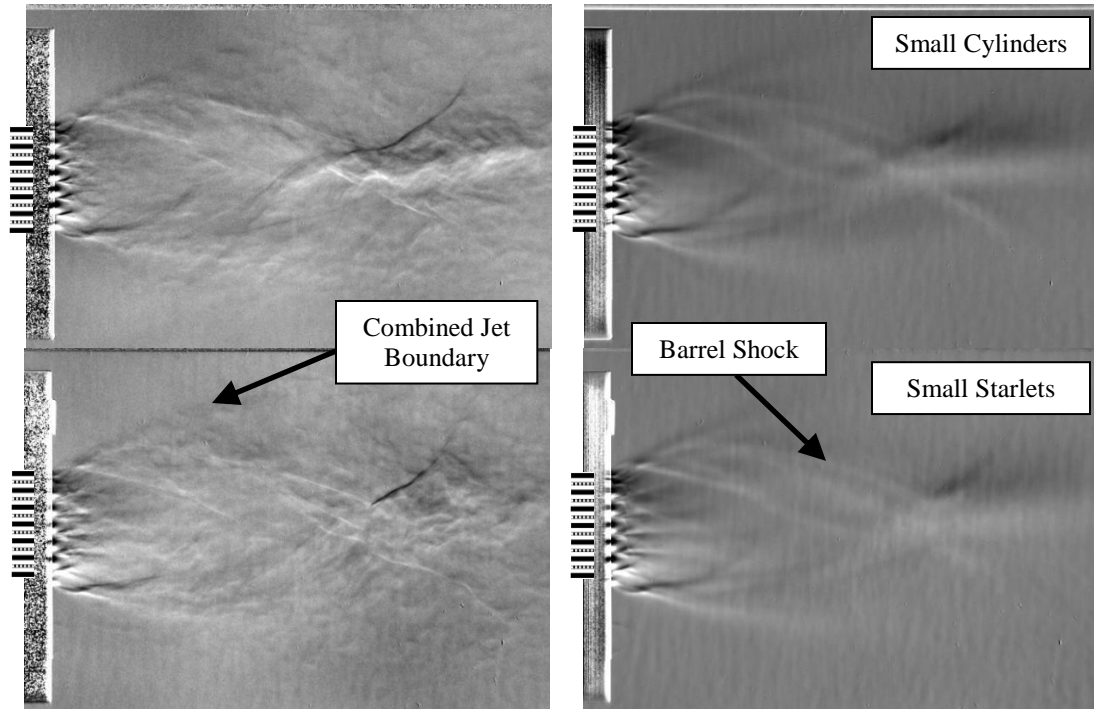


**Figure 11. Small cylinder (top) and starlet (bottom) instantaneous (left) and averaged (right) schlieren images, no injector flow. Image covers an approximate area of 5.5 cm by 8.0 cm.**

Immediately apparent when comparing the small cylinders to the large cylinders is that the small cylinders exhibited an extra row of Prandtl-Meyer expansion fans immediately downstream of the ejector block. While the large ejector geometries exhibited six pairs of fans, the small cylinder geometry had seven. This was simply due to the larger number of ejector exits present, 6 versus 7 for the large and small geometries, respectively, as can be seen in Figs. 1 and 3. It should be noted that while the expansion fan pairs on the bottom of the large ejector geometry images extended significantly further downstream than the top, the pairs downstream of the small ejectors were nearly uniform, suggesting that the exit pressures and velocities across the seven ejectors were nearly uniform; it may be inferred that this was not the case for the large ejectors. The addition of the slot flow also made the top oblique shock of the pair, located approximately 5 cm downstream, visible in the instantaneous image.

The triangle-shaped structures of intersecting weak shocks were steady in time, as evidenced by their clarity in the instantaneous image, and their sharpness in the 200-image average on the right column. As was the case with both large ejector geometries, the addition of the slot flow greatly reduced the size of the downstream intersecting wave structures, widened the barrel shock, and strengthened the oblique shock pair located approximately 5 cm downstream of the ejector face. For brevity, the schlieren images for the 0 mmol/s slot flowrate images were omitted from this paper.

As was the case with the large starlets, the change from small cylinders to starlets reduced the stability of the weak intercepting shock structures, especially in the downstream portion of the flow. This is evidenced by the lowered density gradients of the small starlets as indicated by the reduced sharpness in the averaged images when compared to the small cylinders. Once again, the addition of the slot flow significantly reduced the size of the intersecting wave patterns at the ejector face, as well as reduced the degree to which the flow deviated in an upward direction. Additionally, the barrel shock, both with and without the slot flow present, was wider for the small starlets than it was for the small cylinders. In the case of the starlets, the downstream location of the oblique shock pair once again was closer to the ejector block face, although this was only apparent in the averaged images. The

angle between the oblique weak shocks was consistent with a flow Mach number of approximately 2.1, as deduced by its half angle of approximately 26 degrees.

Figure 12 depicts the schlieren images from the small cylinders and starlets rotated 90 deg. with the same flowrates and row differentiation as Fig. 10.

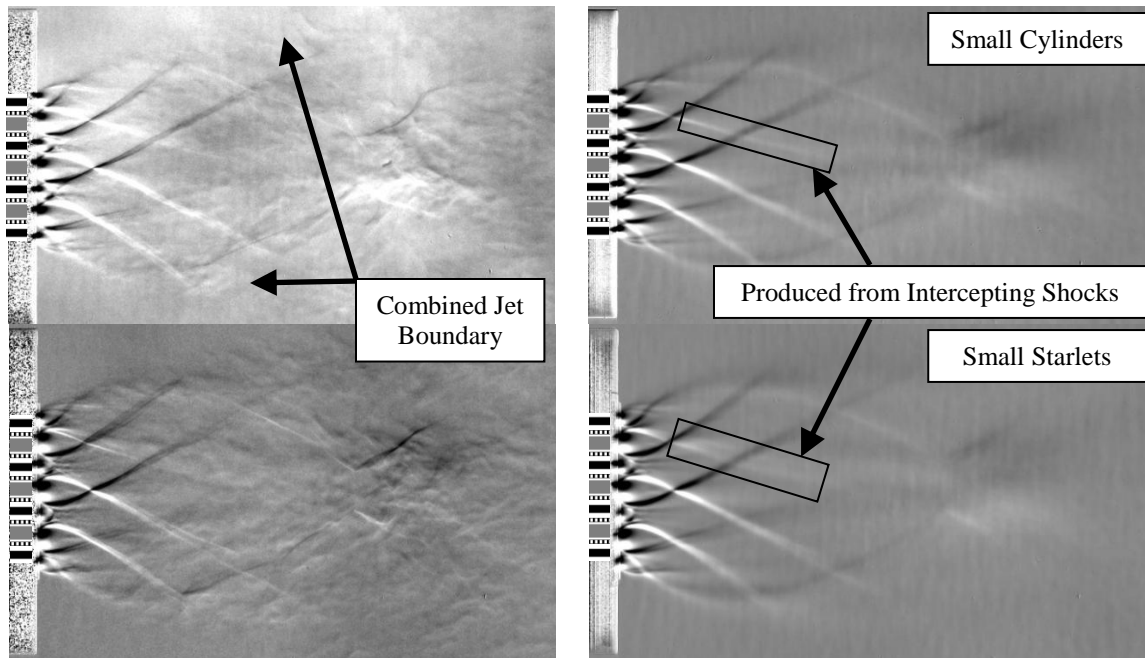


**Figure 12. Small cylinder (top) and starlet (bottom) instantaneous (left) and averaged (right) schlieren images; ejector block rotated 90 degrees, no injector flow. Image covers an approximate area of 5.4 cm by 9.0 cm.**

The differences in flow structure between the large and small cylinders were minor at best. All of the major features were present for both, namely the barrel shocks, oblique shock pair, and the individual weak intercepting shocks of the ejector columns. The weak shocks produced from the intercepting shocks of the ejector-only average flow appear to be less fine, and therefore less stable in time when compared to their large cylinder counterparts, but this may have merely been an artifact of the image contrast difference between the two; once again for the sake of brevity, these images were omitted from this publication.

The addition of starlets to the small cylinders clearly added to the turbulence and instability near the cavity center, presumably enhancing the mixing. This is best substantiated by the observation that without slot flow, the two shockwaves emanating from the inner side of the outer ejector columns move over a wider area with the starlets than with the cylinders, suggesting a small starlet Mach number of 2.0 compared to the small cylinder Mach number of 2.21; this observation was partially obscured when the slot flow was added, which is depicted in Fig. 12.

Comparing the images with the slot and ejector flows present, the oblique shock angle appeared larger for the starlets, and the separation between the two shockwaves was greater, suggesting that the ejector flow had been better mixed with the lower-pressure slot flow, and that a higher mass flow rate existed down the center of the channel, implying that the slot and ejector flows had been more fully mixed with one another, thus bringing more mass to the center of the flow. Reaffirming this hypothesis is the fact that the weak shocks produced from the intercepting shocks were narrower in width and were less fine, which implied better mixing of the ejector flow with that of the slots. These shocks are labeled in Fig. 12, which clearly depicts that these waves remain defined longer and appear to be narrower for the case of the cylinders when compared to the starlets.

## V. Conclusions

Through this set of experiments, it was demonstrated that well-resolved schlieren images may be taken at sub 20 torr pressures if care is taken with the optical setup and if glass, not plastic, windows are used. For this configuration, reducing the ejector flowrate from 686 to 400 to 200 mmol/s yielded weaker interacting structures, but did not significantly change the overall flow structure. Examining the standard orientation images of the

interactions of the slot, ejector, and injector flows, it was observed that the addition of starlets reduced the size and intensity of the observed weak shock and expansion fan structure. Comparing large cylindrical ejectors to their small-diameter counterparts, the large-diameter ejectors displayed stronger expansion fans and shocks; these observations were the same in the case of the large and small starletted ejectors.

The addition of starlets reduced the stability of the expansion fans and widened the barrel shocks and the locations where a Mach disk would be expected to reside. Furthermore, the addition of the starlets appeared to have slowed down the flow, as evidenced by the flow structure not extending as far downstream as that of the cylindrical ejectors, which would be consistent with the enhancement of the mixing of the low and high momentum flows present. For all cases, the addition of the slot flow reduced the size of the weak shock waves structure produced by the individual intercepting shocks, suggesting that the slot flow was being driven into mixing with the injector flows by the ejectors' exit gas expansion; the images from which these observations were made were omitted for the sake of brevity.

Examination of the 90 deg. rotated orientation supported the observations noted from the standard orientation. The density gradients of the downstream oblique shock pair were lowered and the angle between the shocks increased through the addition of starlets, and the weak shocks emanating from the injectors were better defined and extended further downstream for the large ejector cases. It should be noted that when comparing the density gradients visible in the standard orientation, and the 90 deg. rotated orientation, the density gradients viewed in the standard orientation were much less severe than those that were observed in the 90 deg. rotated orientation. For these reasons, it was concluded that to maximize passive mixing in this slot, ejector, and injector arrangement, one must use a larger number of smaller ejectors than a smaller number of large ejectors, and that those ejectors should have starlets located at their exit. Since the interpretation of these schlieren images is highly subjective, further studies should be performed in order to optimize the number of ejectors, weighing the increased convective mixing results against the reduced diffusive mixing that would be expected of a larger ejector exit area.

Recent experimental work by King *et al.*<sup>15</sup> demonstrated that the starlets do in fact significantly improve laser performance with the SEI configuration. These data, along with PLIF visualization data by Ragheb *et al.*<sup>8</sup>, support our conclusions that the starlets enhance the rate of mixing in this multi-stream flow geometry.

### Acknowledgments

We would like to thank the Missile Defense Agency for funding this research effort through a contract with the U.S. Army Space and Missile Defense Command on a Phase II SBIR program with CU Aerospace L.L.C.

### References

- <sup>1</sup>Brown, G., and Roshko, A., "On Density Effects and Large Structure in Turbulent Mixing Layers," *Journal of Fluid Mechanics*, Vol. 64, 1974, pp 775-816.
- <sup>2</sup>Papamoschou, D., and Roshko, A., "The Compressible Turbulent Shear Layer: An Experimental Study," *Journal of Fluid Mechanics*, Vol. 197, 1988, pp. 453-477.
- <sup>3</sup>Yu, K.H., and Schadow, K.C., "Cavity-Actuated Supersonic Mixing and Combustion Control," *Combustion and Flame*, Vol. 99, 1994, pp. 295-301.
- <sup>4</sup>Gilinsky, M.M., and Seiner, J.M., "Corrugated Nozzles for Acoustic and Thrust Benefits," AIAA Paper No. 96-1670, 1996.
- <sup>5</sup>Kim, J.H., and Samimy, M., "Mixing Enhancement via Trailing Edge Modifications in a High Speed Rectangular Jet," *Physics of Fluids*, Vol. 11, 1999, pp. 2731-2742.
- <sup>6</sup>Nikolaev, V.D., and Zagidullin, M.V., "Advanced Nozzle Concepts for the Chemical Oxygen-Iodine Laser (COIL)," EOARD Technical Report of ISTC 22130P-00, 2006.
- <sup>7</sup>Carroll, D.L., and Solomon, W.C., 2005, private communication.
- <sup>8</sup>Ragheb, A.M., Elliott, G.S., Laystrom-Woodard, J.K., King, D.M., Carroll, D.L., and Solomon, W.C., "Low Pressure PLIF Visualization and Mixing Quantification in a Multi-Stream Injection Nozzle," AIAA Paper No. 2010-1439, 2010.
- <sup>9</sup>King D.M., "Experimental Optimization of a Nitrogen-Diluted Chemical Oxygen Iodine Laser," Master's Thesis, Department of Aerospace Engineering, University of Illinois at Urbana-Champaign. Urbana, IL, 2000.
- <sup>10</sup>Nikolaev, V.D., Zagidullin, M.V., Svistun, M.I., Anderson, B.T., Tate, R.F., and Hager, G.D., "Results of Small-Signal Gain Measurements in a Supersonic Chemical Oxygen Iodine Laser With an Advanced Nozzle Bank," *IEEE Journal of Quantum Electronics*, Vol. 38, 2002.
- <sup>11</sup>Settles, G.S., *Schlieren and Shadowgraph Techniques*, Springer-Verlag Publishing, Berlin, Germany, 2001.
- <sup>12</sup>Schetz, J.A., and Billig, F.S., "Penetration of Gaseous Jets Injected into a Supersonic Stream," *AIAA Journal*, Vol. 3, No. 11, 1966, pp. 1658-1665.
- <sup>13</sup>Woodmansee, M.A., and Dutton, J.C., "Experimental Measurements of Pressure, Temperature, and Density in an Underexpanded Sonic Jet Flowfield," AIAA Paper No. 1999-3600, 1999.
- <sup>14</sup>Orescanin, M.M., and Austin, J.M., "Exhaust of Underexpanded Jets from Finite Reservoirs," *AIAA Journal of Propulsion and Power*, to be published, 2010.

<sup>15</sup>King, D.M., Field, T.H., Carroll, D.L., Laystrom-Woodard, J.K., Driscoll, R.J., Sentman, L.H., "Performance of a Multi-Stream Injection COIL with Starlet Ejectors," AIAA Paper No. 2010-4754, 2010.